Journal of Alloys and Compounds 522 (2012) 172–177

Contents lists available at SciVerse ScienceDirect

Journal of Alloys and Compounds

journal homepage: www.elsevier.com/locate/jallcom

Optical properties change in $Sb_{40}S_{40}Se_{20}$ thin films by light-induced effect

Ramakanta Naik[a,b,*], Sanjit K. Parida[a], C. Kumar[a], R. Ganesan[a], K.S. Sangunni[a]

[a] Indian Institute of Science, Bangalore 560012, India
[b] APEX Institute of Technology, Bhubaneswar 752101, India

ARTICLE INFO

Article history:
Received 30 October 2011
Accepted 26 January 2012
Available online 3 February 2012

Keywords:
Chalcogenides
Thin films
Optical properties
FTIR
XPS

ABSTRACT

Thin films of $Sb_{40}Se_{20}S_{40}$ with thickness 1000 nm were prepared by thermal evaporation technique. The amorphous nature of the thin films was verified by X-ray diffractometer. The chemical composition of the deposited thin films was examined by energy dispersive X-ray analysis (EDAX). The changes in optical properties due to the influence of laser radiation on amorphous thin films of $Sb_{40}Se_{20}S_{40}$ glassy alloy were calculated from absorbance spectra as a function of photon energy in the wavelength region 450–900 nm. Analysis of the optical absorption data shows that the rule of non-direct transitions predominates. It has been observed that laser-irradiation of the films leads to a decrease in optical band gap while increase in absorption coefficient. The decrease in the optical band gap is explained on the basis of change in nature of films due to disorderness. The optical changes are supported by X-ray photoelectron spectroscopy and Raman spectroscopy.

1. Introduction

Chalcogenide glasses are inorganic materials which contain one or more of the chalcogen elements: S, Se or Te in conjunction with any (more) electropositive elements of group V of the periodic table. These glasses are generally semiconductors, opaque in the visible region of the spectrum and chemical bonding of the matrix is usually directional and covalent. Because of their interesting application as electronic and optical materials a great amount of work in recent years has been expended. Studies of amorphous chalcogenide glasses are of considerable interest due to their importance in preparing electronic memories and their optical applications as good IR transmitting materials [1,2]. Recent applications of chalcogenide glasses in the field of optics include the optical imaging, optical data storage, integrated optics and infrared optics due to their excellent transmittance reaching the far-infrared spectral region effects. Among them, metal chalcogenide semiconductors of the V–VI group have received considerable attention because of their interesting physical properties as well as their potential application in optoelectronic, thermoelectric and photoelectric devices [3–5]. The importance of these materials arises from that they generally offer a wide range of optical, electrical, and structural properties.

Among these compounds, Sb_2S_3 and Sb_2Se_3 are important photoconductive semiconductors (E_g) 1.64 and 1.11 eV, respectively) that crystallize in the orthorhombic system [6,7]. Their useful properties (e.g., photovoltaic, photo conducting, photo catalytic, Peltier effect) make them promising candidates for important applications in diverse areas such as solar energy conversion, thermoelectric cooling, photo detector technology, thermoelectric power generation, and optoelectronics in the near-infrared region [8,9]. Sb_2Se_3 has received a great deal of attention due to its switching effects and its excellent photovoltaic properties and high thermoelectric power, which could find potential applications in solar selective and decorative coating, optical and thermoelectric cooling devices [10]. On the other hand, Sb_2S_3 has attracted attention for its applications as a target material for television cameras, as well as in microwave, switching, and optoelectronic devices. So, both Sb_2S_3 and Sb_2Se_3 have potential applications in various fields. By making suitable solid solutions among them, it is possible to obtain a new alloy with specific characteristics to meet a desired requirement. In the present system, we have incorporated Sb in the Se–S system. The addition of third element creates compositional and configurationally disorder in the system.

Photo-induced changes in amorphous chalcogenides are an object of systematic investigations with a view to better understanding the mechanisms of the phenomena taking place in them as well as their practical applications. It is well established that chalcogenide glasses undergo structural changes under the action of external influences such as laser, neutron, electron and gamma irradiation [11–17]. Chalcogenide materials also have the important property that, although there are some gap states, they do not carry the traditional electron spin resonance (ESR) defect signature of unpaired spins. The lone-pair character of the valence tails leads to very rich behavior under the influence of light. The knowledge

* Corresponding author. Tel.: +91 80 22932716; fax: +91 80 23602602.
E-mail addresses: ramakanta@physics.iisc.ernet.in, ramakanta.naik@gmail.com (R. Naik).

0925-8388/$ – see front matter © 2012 Elsevier B.V. All rights reserved.
doi:10.1016/j.jallcom.2012.01.144

of the optical properties of thin films is very important in many scientific, technological and industrial applications of thin films such as photo-conductivity, solar energy, photography, and numerous other applications. The study of the optical absorption spectra in chalcogenide glasses provides essential information about the band structure and the energy band gap. The optical band gap of the material plays a major role in the preparation of the device for a particular wavelength, which can be modified by the addition of impurity [18]. So, the influence of metallic additives on the optical properties has been an important issue in the case of chalcogenide glasses.

The present communication reports the effect of laser irradiation on optical properties of amorphous thin films of $Sb_{40}Se_{20}S_{40}$. The optical properties such as optical band gap, Tauc parameter, Urbach energy have been derived from transmission spectra, at normal incidence, in the 400–1200 nm spectral range. Raman and X-ray photoelectron spectroscopy (XPS) were also carried out to support the optical changes.

2. Experimental

Bulk glass of $Sb_{40}Se_{20}S_{40}$ was prepared by melt quenching technique. Materials of (99.995% pure) S, Se and Sb were weighed according to their atomic percentage and sealed in a quartz ampoule in a vacuum of $\sim 10^{-5}$ Torr. The sealed ampoule was kept inside a rotating furnace at 950 °C for 36 h to make the melt homogeneous. The bulk glass was obtained by quenching the ampoule in ice cooled water. Thin films were prepared by thermal evaporation method at a base pressure of 1×10^{-5} Torr from the prepared bulk glass onto the glass substrates (microscope slides). During the deposition process (at normal incidence), the substrates were suitably rotated in order to obtain the films of uniform thickness. The thicknesses of the films were around 1000 nm. The elemental composition of the as-prepared film was checked by energy dispersive X-ray analysis (EDAX) in Sirion XL 40 in which EDAX is attached. The scan was done at 20 kV with 40 μA emission current exposing a sample of 1 cm^2 size at 2×10^{-7} Torr pressure. The estimated average precision was less than 5% in atomic fraction in each element. The amorphous state of the film was checked by X-ray (Philips type 1710 with Cu as target and Ni as filter, λ = 1.5418 Å) diffractometer (XRD). To study the photo-induced changes, we irradiated the film at room temperature by a diode pumped solid state laser (DPSS) of wavelength 532 nm with a power of 40 mW. The film was mounted on a sample holder and the laser light was focused into 2 mm wide spot. The optical absorption spectra of the as-prepared and illuminated films were taken by using the Fourier transform infrared (FTIR) spectrometer (Bruker Optics (IFS66v/S)) in the visible wavelength range of 400–1200 nm at room temperature. We have used XPS to analyze the new bonds formed due to photo-induced effect. It is a useful surface analytical technique to study the chemical state and local environment of an atom. The XPS core level spectra were obtained with monochromatic Mg Kα X-rays (1253.6 eV) at a vacuum of 10^{-9} Torr in Multilab 2000 Thermo Scientific UK instrument. The XPS data consisted of survey scans over the entire binding energy (BE) and selected scans over the core level peaks of interest. An energy increment of 1 eV was used for recording the survey spectra and 0.05 eV for the case of core level spectra. The core level peaks were recorded by sweeping the retarding field and using the constant pass energy of 30 eV. The data were averaged over three scans. The reproducibility of the measurements was checked on different regions of the investigated surfaces. For insulators such as glasses, the charging effect can change the BE of the electrons from sample to sample. Hence, the measurement of the absolute BE of electrons from a specified energy level is not reliable. The C 1s line from either adventitious carbon or intentionally added graphite powder on the surface has been widely used for charge referencing [19,20]. For this study, the adventitious carbon was used as a reference and the BE of the reference C 1s line was set as 284.6 eV. For each sample, a calibration factor was calculated from the difference between the measured C 1s BE and the reference value 284.6 eV [21]. The original BE data were corrected according to the calibration factor. The room temperature Raman spectra were recorded in the 180° backscattering geometry, using a 532 nm excitation from a diode pumped frequency doubled Nd–YAG solid state laser and a custom built Raman spectrometer equipped with SPEX TRIAX 550 monochromator and a liquid nitrogen cooled CCD. Laser power at the sample was ~15 mW and a typical spectrum acquisition took ~1–2 min.

3. Results and discussions

The X-ray diffraction patterns, taken at room temperature for both as-prepared and laser irradiated thin films are shown in Fig. 1. The absence of sharp structural peaks for both the thin films confirms the amorphous nature of the samples. The width of 2θ was

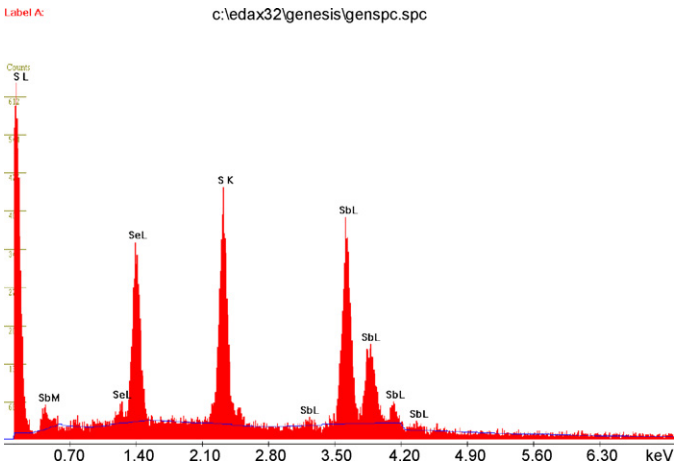

Fig. 1. XRD patterns of the $Sb_{40}Se_{20}S_{40}$ thin films.

Table 1
The measured elemental composition from EDAX for $Sb_{40}Se_{20}S_{40}$ thin film.

Element	Wt%		At%	
	Observed	Calculated	Observed	Calculated
S	16.35	16.58	39.18	40
Sb	60.25	62.98	38.04	40
Se	23.40	20.44	22.78	20
Total	100.00	100	100.00	100.00

from 23° to 35°. The diffractograms are very similar to the point that no differences can be recorded between the two films. The EDAX results from the $Sb_{40}Se_{20}S_{40}$ films listed in Table 1 confirm the presence of Se, S and Sb in the as-deposited films and reveal nearly stoichiometric compositions. The spectrum is shown in Fig. 2.

The transmittance spectra of both the films as a function of wavelength are plotted in Fig. 3. It can be seen that the 'non-shrinking' interference fringes observed in the transmittance spectra at higher wavelength (500–1100 nm) indicate the homogeneity and smoothness of the deposited films. Furthermore, the absorption edge of the deposited film shows a blue shift when the film was illuminated. This shift indicates the reduction of the optical band gap of the illuminated film. The absorption coefficient of the $Sb_{40}Se_{20}S_{40}$ thin films was calculated from the experimental data

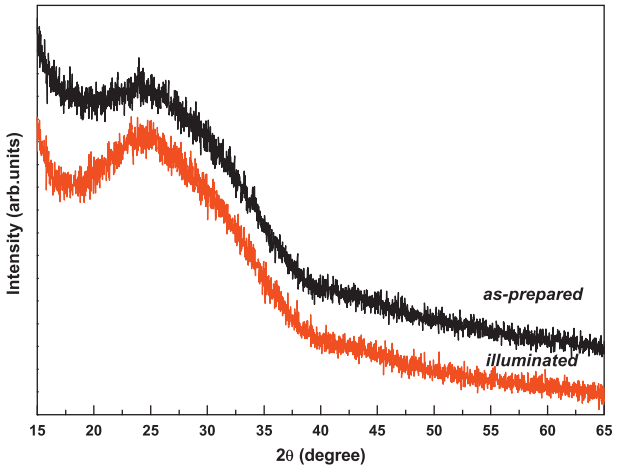

Fig. 2. EDAX spectrum of the $Sb_{40}Se_{20}S_{40}$ thin film.

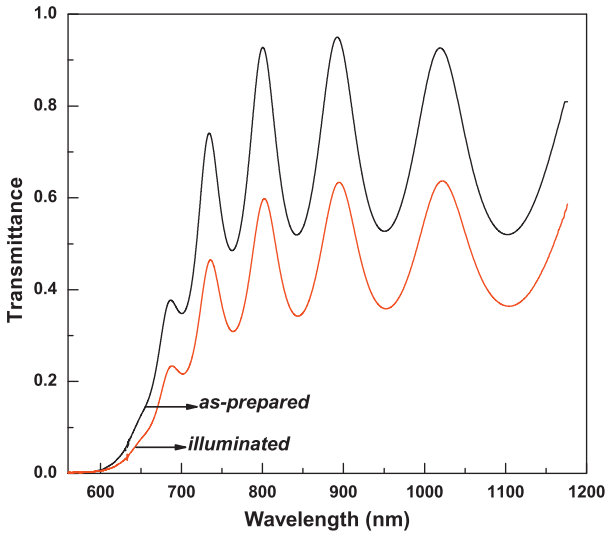

Fig. 3. Transmission spectra of the $Sb_{40}Se_{20}S_{40}$ thin films.

of transmittance and reflectance in the strong absorption region using the relation [22]

$$\alpha = \left(\frac{1}{d}\right) \ln\left(\frac{(1-R)^2}{T}\right) \quad (1)$$

where T is the transmittance, R is the reflectance and d is the thickness of the deposited film. Fig. 4 shows the dependence of the absorption coefficient on wavelength for the amorphous thin films. It has been observed that the absorption coefficient increases with laser irradiation. In crystalline materials, the fundamental edge is directly related to transitions from the conduction and valence band, and associated with direct and indirect band gaps, whereas in the case of amorphous material the transitions are termed non-direct owing to the absence of an electronic band structure in k-space. In the absorption process, a photon of known energy excites an electron from a lower to a higher energy state, corresponding to an absorption edge. In chalcogenide glasses, a typical absorption edge can be broadly ascribed to one of the three processes: (i) Residual below-gap absorption (ii) Urbach tails and (iii) interband absorption.

Chalcogenide glasses have been found to exhibit highly reproducible optical edges, which are relatively insensitive to preparation conditions and only the observable absorption [23] with a gap under equilibrium conditions account for the first

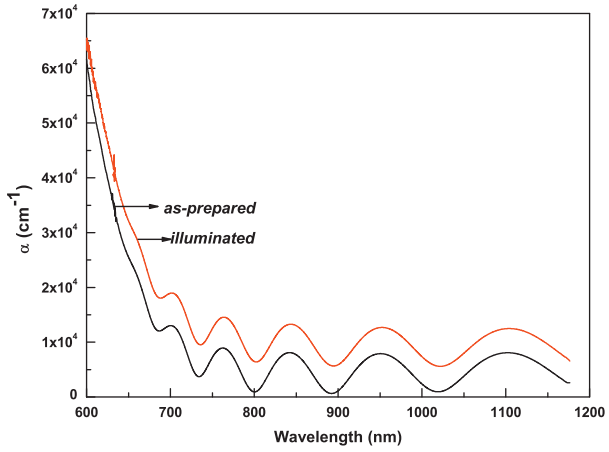

Fig. 4. (vs λ for the $Sb_{40}Se_{20}S_{40}$ thin films.

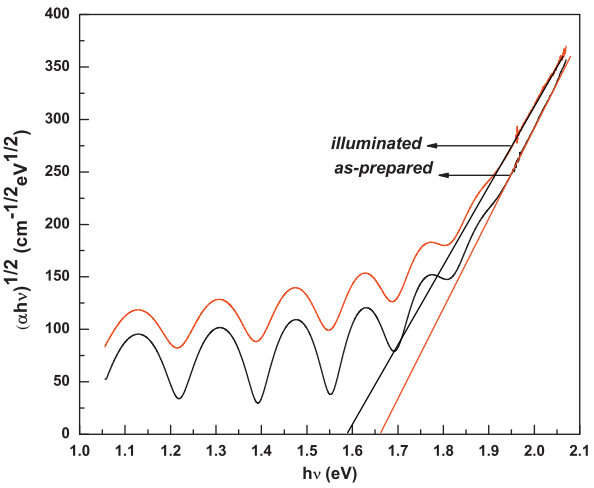

Fig. 5. ($(h()^{1/2}$ vs ($h($) plots for the $Sb_{40}Se_{20}S_{40}$ thin films.

process. In amorphous materials, a different type of optical absorption edge is observed and absorption coefficient increases exponentially with the photon energy near the energy gap. This type of behavior has also been observed in other chalcogenides [24,25]. This optical absorption edge is known as the Urbach edge and is given by,

$$\alpha(h\nu) = \alpha_0 \exp\left(\frac{h\nu}{E_e}\right) \quad (2)$$

where α_0 is a constant and E_e corresponds to the Urbach energy (the width of the band tail of the localized states in the band gap). In this region, transition between (defect) states in the gap and the bands take place [26]. Plotting the dependence of log (α) on photon energy will give a straight line. The calculated value of E_e, the inverse of the slope of the straight line, gives the width of the tails of the localized states into the gap at band edges.

The fundamental absorption edge in most amorphous semiconductors follows an exponential law. Above the exponential tail, the absorption coefficient has been reported [23] to obey the following equation:

$$(\alpha h\nu)^{1/m} = B(h\nu - E_g) \quad (3)$$

where ν is the frequency of the incident beam, B is a constant, E_g is optical band gap and m is an exponent, which can be assumed to have values of 1/2, 3/2, 2 and 3 depending on the nature of electronic transition responsible for the absorption: $m = 1/2$ for allowed direct transition, $m = 3/2$ for forbidden direct transition, $m = 2$ for allowed indirect transition and $m = 3$ for forbidden indirect transition [27]. The best fit of the experimental results of as-prepared and irradiated thin films of $Sb_{40}Se_{20}S_{40}$ using Eq. (3), with $m = 2$ i.e., the variation curve of $(\alpha h\nu)^{1/2}$ with photon energy ($h\nu$) for amorphous and laser irradiated thin films of $Sb_{40}Se_{20}S_{40}$ (shown in Fig. 5) is found to be identical to that of the elemental amorphous semiconductor [28,29]. This indicates that the absorption in as-prepared and irradiated thin films of $Sb_{40}Se_{20}S_{40}$ is due to non-direct transition. Plotting the dependence of $(\alpha h\nu)^{1/2}$ on photon energy ($h\nu$) will give a straight line and the y intercept gives the value of the optical band gap (Fig. 5). The slope of the fitting gives $B^{1/2}$. The constant B includes information on the convolution of the valence band and conduction band states and on the matrix element of optical transitions, which reflects not only the k selection rule but also the disorder-induced spatial correlation of optical transitions between the valence band and conduction band [24]. Moreover, B is highly dependent on the character of the bonding. The reflection loss was not that much as compared to the high absorption in the band gap region.

The optical band gaps of the as-prepared and the illuminated films are found to be 1.66 eV and 1.59 eV, respectively. Since, the optical absorption depends on short-range order in the amorphous states and defects associated with it, the decrease in optical band gap may be explained on the basis of "density of state model" proposed by Mott and Davis [30]. According to this model, the width of the localized states near the mobility edges depends on the degree of disorder and defects present in the amorphous structure. In particular, it is known that unsaturated bonds together with some saturated bonds are produced as the result of an insufficient number of atoms deposited in the amorphous film [31]. The unsaturated bonds are responsible for the formation of some of the defects in the films, producing localized states in the amorphous solids. The presence of high concentration of localized states in the band structure is responsible for the decrease of optical band gap in the case of the amorphous films. This decrease in the band gap may also be due to the shift in Fermi level, whose position is determined by the distribution of electrons over the localized states [32]. The decrease in optical band gap (E_g) with laser irradiation can be attributed to the reduction in the density of tail states adjacent to the band edge.

The $B^{1/2}$ values for as-prepared and illuminated films are 687 and 598 $cm^{-1/2}\,eV^{-1/2}$, respectively. The $B^{1/2}$ for illuminated film is less than the as-prepared film which indicates the presence of more no of homopolar bonds due to disorder. It is known that the Urbach edge is a useful parameter to evaluate the degree of disorder. The value of E_e for as-prepared and illuminated $Sb_{40}Se_{20}S_{40}$ films is 243 meV and 289 meV, respectively. The Urbach energy E_e of the illuminated film is more than that of as-prepared film which indicates the increase in chemical disorder after illumination. The lower values of $B^{1/2}$ and higher values of E_e of the illuminated film over the as-prepared film clearly indicate that the illuminated film is more disordered (chemically) than the as-prepared film, i.e., the creation of homopolar bonds after photo-induced process.

The changes in the full transmission spectra for as-prepared and laser irradiated thin films of $Sb_{40}Se_{20}S_{40}$ are compared in Fig. 3. The shift of the interference interval arises because of the change in the film thickness and/or refractive index. We calculated the film thickness by fitting the transmission $T(\lambda)$ curve according to the Swanepoel model [33]. The relative changes in the film thickness ($\Delta d/d$, <1%) are small. Generally speaking, a decrease in the band gap (red shift in the absorption edge) is accompanied by a increase in the refractive index according to Moss's rule ($E_g n^4 \sim$ constant) [34]. The refractive index n can be obtained by fitting the transmission $T(\lambda)$ curve according to the Swanepoel theory. The refractive index (n) is obtained using the following expressions,

$$n = [M + (M^2 - s^2)^{1/2}]^{1/2} \quad (4)$$

$$\text{where} \quad M = \left[\frac{2s}{T_m}\right] - \left[\frac{(s^2+1)}{2}\right] \quad (5)$$

for transparent region and

$$M = \left[2s\left(\frac{T_M - T_m}{T_M T_m}\right)\right] + \left[\frac{(s^2+1)}{2}\right] \quad (6)$$

for weak and medium absorption region.

'T_M' and 'T_m' are the maximum and minimum transmission values at a particular wavelength, 's' is the refractive index of the substrate. Refractive index is obtained by extrapolating envelops corresponding to T_M and T_m. The fringes are used to calculate the refractive index (n) of the thin films using Eqs. (4)–(6). The refractive index is found to decrease with the increase in wavelength and due to irradiation it increased (Fig. 6). The photo-induced change that is accompanied by a decrease in the film thickness (photo contraction, Table 1) and thus a increase in the density of the exposed

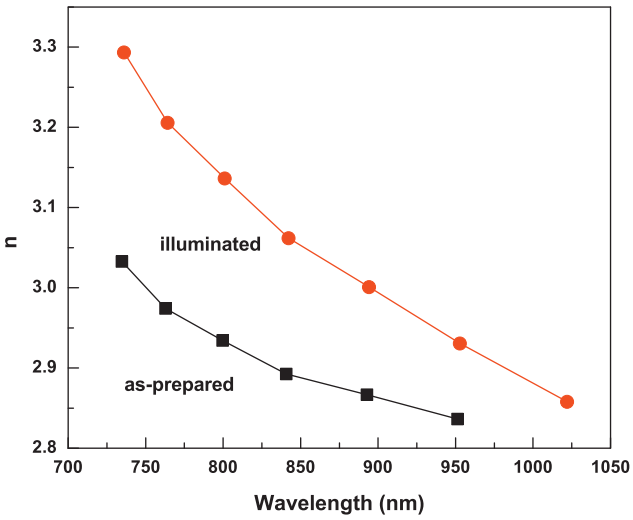

Fig. 6. Variation of n with λ for the $Sb_{40}Se_{20}S_{40}$ thin films.

region is responsible for the observed increase in the refractive index [34].

A typical XPS spectrum of $Sb_{40}Se_{20}S_{40}$ film contains many photoelectrons and Auger peaks of S, Se and Sb. But, we have considered only the core peaks such as S 2p, Sb 4d, Se 3d and Se 3p for the present study. The Se 3d spectra of the as-prepared and illuminated films are shown in Fig. 7. The Se 3d peak position for as-prepared and illuminated films is at 54.37 and 54.87 eV, respectively. The peak shifts toward higher BE shows the formation of Se–Se homopolar bonds due to illumination. The peak position of Sb 4d core level spectra (Fig. 8) for as-prepared and illuminated films is at 33.76 and 33.44 eV, respectively. It is found that the peak is shifting toward the lower BE due to the formation of more Sb–Sb homopolar bonds. The pure Se $3p_{3/2}$ (161.7 eV) and S 2p (164 eV) peaks are close to each other. So, we have deconvoluted the peak to distinguish from each other as shown in Fig. 9(a and b). From the spectra of S 2p peak, it is found that due to illumination, the peak is shifting toward the higher BE due to the formation of S–S homopolar bonds. The S 2p peak position for as-prepared and illuminated films is at 163.01 and 163.36 eV, respectively. The intensity of the S 2p peak increased with illumination shows the formation of more homopolar bonds. This is well supported by the Raman spectra where we can also see the increase in S–S vibrational mode

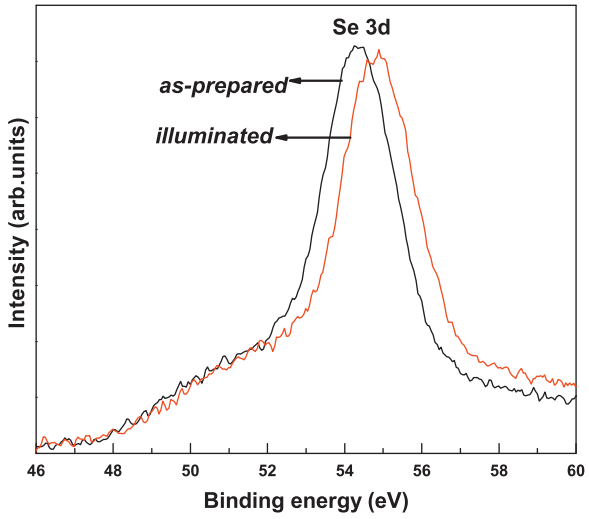

Fig. 7. XPS core level spectra of Se 3d of the $Sb_{40}Se_{20}S_{40}$ thin films.

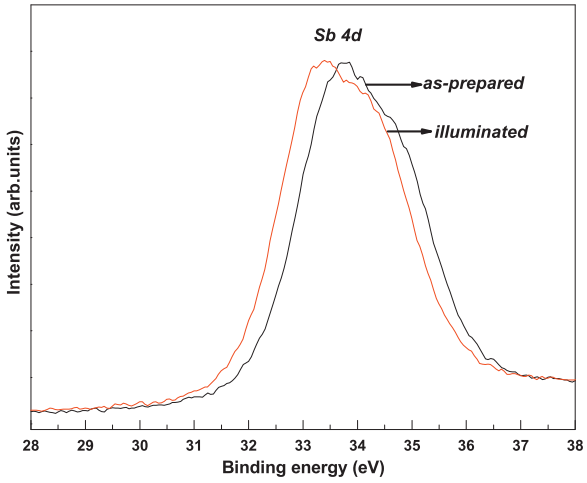

Fig. 8. XPS core level spectra of Sb 4d of the $Sb_{40}Se_{20}S_{40}$ thin films.

at 450 cm^{-1} due to illumination (discussed below). There is also shift in the position of Se 3p peaks due to illumination process. But, due to the weak signal (Se 3d is the outer most core level in Se), we cannot discuss much about that. This is in accordance with

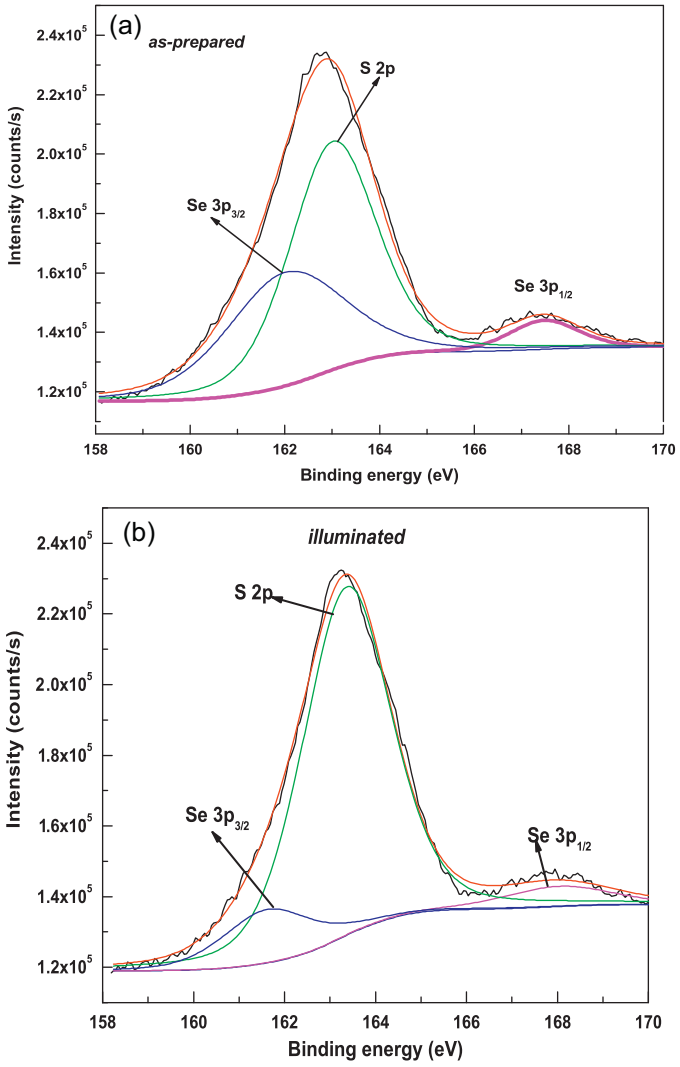

Fig. 9. XPS core level spectra of S 2p and Se 3p of the $Sb_{40}Se_{20}S_{40}$ thin films.

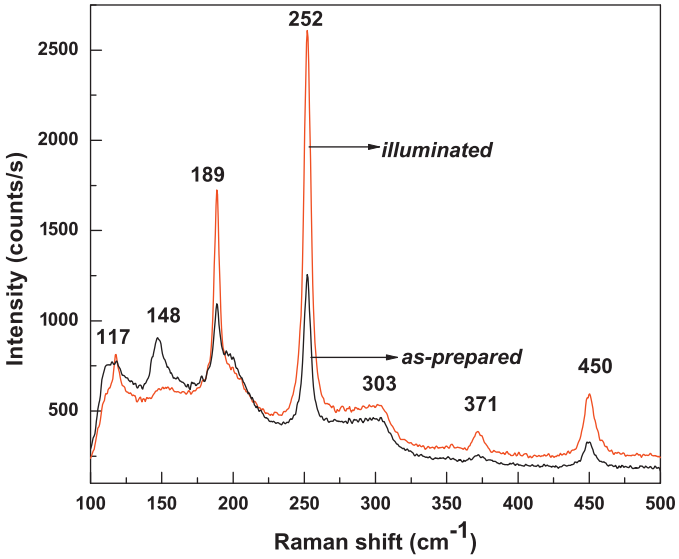

Fig. 10. Raman spectra of the $Sb_{40}Se_{20}S_{40}$ thin films.

the reduction in optical band gap of the as-prepared film due to photo-induced process.

Direct evidence of structural changes in $Sb_{40}Se_{20}S_{40}$ thin films caused by illumination was obtained from Raman spectra (Fig. 10). According to the molecular model [35], each Sb atom in the Sb–Se–S ternary compound is covalently bonded to three Se atoms in a pyramidal unit ($Sb–Se_3$), and also covalently bonded to three S atoms in a pyramidal unit ($Sb–S_3$). The basic structural units $SbSe_3$ and SbS_3 are interconnected through bridging S atoms. The coupling between the basic structural groups via S atoms is assumed to be weak, and the vibrational modes are separated into $SbSe_3$ and SbS_3 like modes. The $Sb_{40}Se_{20}S_{40}$ thin films have an over stoichiometry of metal atoms (Sb), and some Sb–Sb bonds should be present in the alloy too. The peak at 148 cm^{-1} represents the Sb–Sb vibrations. The SbS_3 pyramidal vibrational mode is developed at 303 cm^{-1} in the neighborhood of the dominant vibrational band of $SbSe_3$ at 252 cm^{-1} in the Raman spectra. It is clear that the band at 303 cm^{-1} is due to the Sb–S vibration in $Sb–S_3$, (S_2) Sb–Sb (S_2) and the band at 252 cm^{-1} is due to the Sb–Se vibration in $Sb–Se_3$, (Se_2) Sb–Sb (Se_2). The peak at 117 cm^{-1} corresponds to disulfide bonds S–S (or two membered S^2 chains) in $S_2Sb–S–S–SbS_2$ vibration. The peak at position 450 cm^{-1} in the spectra may due to formation of S–S bonds. The peak at 189 cm^{-1} corresponds to diselenide bonds Se–Se (or two membered Se^2 chains) in $Se_2Sb–Se–Se–SbSe_2$ vibration. The peak at 371 cm^{-1} corresponds to the formation of Sb–Sb vibrations. The peak intensity at 117, 189, 371 and 450 cm^{-1} increased with illumination suggesting the formation of more no of homopolar bonds. The increase in intensity at 252 cm^{-1} suggests the modifications in $SbSe_3$ vibrational band where as there is no change in the SbS_3 vibrational mode at 303 cm^{-1}. The changes in the different vibrational modes of the Raman spectra clearly supports the optical changes occurred due to illumination.

4. Conclusions

In conclusion, thermally evaporated amorphous thin films undergo structural transformations when exposed to band gap illumination (photo-structural transformations). Photo-induced changes of optical transmissivity, optical band gap, $B^{1/2}$, Urbach energy takes place due to illumination process. The decrease in optical band gap is due to the change in localized states near to the band edges. The binding energy shift of different core level spectra shows the formation of more homopolar bonds which

supports the decrease in optical band gap. The change in intensity of Raman spectra supports the optical changes due to illumination. So, the photo-induced changes can be assigned to chemical bond redistribution.

Acknowledgments

The authors thank DST for using the National Facility for Optical Spectrometry at Department of Physics and Surface Science facility, IISc for XPS measurement.

References

[1] S. Surinach, N. Clavaguera, M.D. Baro, Mater. Sci. Eng. 97 (1998) 533.
[2] E.A. Marseglia, E.A. Davis, J. Non-Cryst. Solids 50 (1982) 13.
[3] M.J. Chokalingam, K. Nagarajo Rao, R. Rangarajan, C.V. Suryanarayana, J. Phys. D: Appl. Phys. 3 (1970) 629.
[4] B. Roy, B.R. Chakraborty, R. Bhattacharya, A.K. Dutta, Solid State Commun. 25 (1978) 617.
[5] P.K. Nair, M.T.S. Nair, V.M. Garcı a, O.L. Arenas, Y. Pena, A. Castillo, I.T. Ayala, O. Gomez Daza, A. Sanchez, J. Campos, H. Hu, R. Sua rez, M.E. Rincon, Solar Energy Mater. Solar Cells 52 (1998) 313.
[6] X.W. Zheng, Y. Xie, L.Y. Zhu, X.C. Jiang, Y.B. Jia, Y.P. Sun, Inorg. Chem. 41 (2002) 455.
[7] Y. Yu, R.H. Wang, Q. Chen, L.M. Peng, J. Phys. Chem. B 110 (2006) 13415.
[8] R.N. Bhattacharya, P. Pramanik, Solar Energy Mater. 6 (1982) 317.
[9] I. Kim, Mater. Lett. 43 (2000) 221.
[10] K.Y. Rajapure, C.D. Lokhande, C.H. Bhosele, Thin Solid Films 311 (1997) 114.
[11] P. Lucas, E.A. King, A.D. Horner, B.R. Johnson, S.K. Sundaram, J. Non-Cryst. Solids 352 (2006) 2067.
[12] N.A. Elalaily, R.M. Mahamed, J. Nucl. Mater. 303 (2002) 44.
[13] M.M.A. Imran, N.S. Saxena, Y.K. Vijay, R. Vijayvergiya, N.B. Maharjan, M. Husain, J. Non-Cryst. Solids 298 (2002) 53.
[14] S.M. El-Sayed, Nucl. Instrum. Methods B 225 (2004) 535.
[15] M.M.A. Imran, I.F. Al-Hamarneh, M.I. Awadallah, M.A. Al-Ewaisi, Physica B 403 (2008) 2639.
[16] R. Golovchak, O. Shpotyuk, A. Kozdras, B. Bureau, M. Vlcek, A. Ganjoo, H. Jain, Philos. Mag. 87 (2007) 4323.
[17] R. Ya Golovchak, A. Kozdras, Cz Gorecki, O.I. Shpotyuk, J. Non-Cryst. Solid 352 (2006) 4960.
[18] E. Marquez, T. Wagner, J.M. Gonzalez-Leal, A.M. Bernal-Olive, R. Prieto-Aleon, R. Jimenez-Garay, P.J.S. Ewen, J. Non-Cryst. Solids 274 (2000) 62.
[19] M.D. Mikhailov, E.A. Karpova, Z. Cimpl, F. Kosek, Phys. Status Solidi A 117 (1990) 467.
[20] J.F. Moulder, W.F. Sticker, P.E. Sobol, K.D. Bomben, Hand Book of X-ray Photoelectron Spectroscopy, Perkin Elmer, Eden Pairie, MN, 1992.
[21] T.L. Barr, S. Seal, J. Vac. Sci. Technol. A 13 (1995) 1239.
[22] A.A. Othman, M.A. Osman, H.H. Amer, A. Dahshan, Thin Solid Films 457 (2004) 253.
[23] M. Abkowitz, Polym. Eng. Sci. 24 (1984) 1149.
[24] J. Tauc, in: J. Tauc (Ed.), Amorphous and Liquid Semiconductors, Plenum Press, New York, 1979, p. 159.
[25] F. Urbach, Phys. Rev. 92 (1953) 1324.
[26] S.R. Elliot, Materials Science and Technology: A Comprehensive Treatment, Wiley, New York, 1991, p. 376.
[27] R.A. Smith, Phil. Mag. Suppl. 2 (1953) 81.
[28] A. Ahmad, S.A. Khan, L. Kumar, Z.H. Khan, M. Zulfequar, M. Husain, Vacuum 82 (2008) 608.
[29] S.A. Khan, M. Zulfequar, M. Husain, Curr. Appl. Phys. 5 (2005) 583.
[30] N.F. Mott, E.A. Davis, Electronics Processes in Non-Crystalline Materials, Clarendon, Oxford, 1979, p. 428.
[31] M.L. Theye, Proceedings of the Vth International Conference on Amorphous and Liquid Semiconductors 1, 1973, p. 479.
[32] T.T. Nang, M. Okuda, T. Matsushita, S. Yokota, A. Suzuki, Jpn. J. Appl. Phys. 14 (1976) 849.
[33] R. Swanepoel, J. Phys. E Sci. Instrum. 16 (1983) 1214.
[34] P. Knotek, L. Tichy, D. Arsova, Z.G. Ivanova, H. Ticha, Mater. Chem. Phys. 119 (1–2) (2009) 315.
[35] G. Lucovsky, R.M. Martin, J. Non-Cryst. Solids 8–10 (1972) 185.